Optik - International Journal for Light and Electron Optics 208 (2020) 163535

Contents lists available at ScienceDirect

Optik

journal homepage: www.elsevier.com/locate/ijleo

Original research article

Accurate estimation of transmission maps for image restoration based on polarimetric parameters and average intensity

Yongnan Lu[a,b], Mingfei Xu[a], Shuqiang Jia[a], Yunda Zheng[a,b], Xiaofei Zhang[a,b], Wei Huang[a,*]

[a] State Key Laboratory of Applied Optics, Changchun Institute of Optics, Fine Mechanics and Physics, Chinese Academy of Sciences, Changchun, 130033, China
[b] University of Chinese Academy of Sciences, Beijing, 100049, China

ARTICLE INFO

Keywords:
Polarimetric imaging
Imaging through turbid media
Image enhancement

ABSTRACT

Haze limits visibility and degrades image contrast, and images lose color fidelity owing to the scattering and absorption of light caused by particles. Consequently, removing haze is critical for enhancing the image visibility and quality, with estimation of airlight and transmission map being critical steps. We propose a simple and convenient improved scheme, which is polarization-based method for dehazing. The method uses four polarization orientations (0°, 45°, 90°, 135°) to measure the Stokes vector, and obtained the degree of polarization (DOP) of the airlight by angle of polarization (AOP) in three channels. Subsequently, estimating the airlight at infinity by average total intensity and re-constructing a matrix to estimate the transmission maps. Experimental results demonstrate that a high-quality transmission map can be obtained, and this improved method can restore outdoor scene haze images with high quality and contrast. In addition, this method also proved to be useful for enhancing color saturation and restoring color fidelity.

1. Introduction

Image quality is compromised by a turbid medium (e.g., particles, water drops, fog, rain, snow, and haze) which introduces scattering and absorption; consequently, object irradiance detectors exhibit attenuated visibility and low contrast. Thus, it is important to obtain detailed information, increase the object visibility, and recover real color in such conditions. Dehazing methods fall into two categories: those that utilize polarimetric images [1–9] and those that use computer vision techniques [5,10–18]. These two types of dehazing methods always depend on the atmospheric scattering model, but dehaze images differently. Both approaches have merits and drawbacks. Computer vision-based methods require strong prior knowledge and assumptions to enhance visibility based on one image [18]. Polarimetric methods always utilize multiple images (e.g., 0°, 45°, 90°, and 135° orientations) to estimate atmospheric light at infinity and medium transmittance. On one hand, computer vision-based methods use only one image, while polarimetric image methods require at least two images; thus, polarization-based methods cannot be used in real time. On the other hand, computer vision-based methods depend on external knowledge about the scene's structure or aerosols [17]; thus, it is very important to accurately estimate these parameters. This approach cannot be used on high-brightness targets [8]. To acquire accurate transmission maps, computer vision-based methods use the technique of matting, but recovered images contain halo artifacts in some cases. Polarization-based methods always depend on the sky region to estimate airlight, but this approach fails when images contain

* Corresponding author.
E-mail address: huangw@ciomp.ac.cn (W. Huang).

https://doi.org/10.1016/j.ijleo.2019.163535
Received 3 July 2019; Accepted 2 October 2019

no sky regions. To acquire high-quality dehazed images, these two types of methods incorporate complicated procedures that increase the computation time.

In this paper, we propose a improving method to dehazing of images based on polarimetric information, which is based on the Stokes vectors. The underlying principle of our algorithm is simple. First, we acquire four polarimetric images (0°, 45°, 90°, and 135°) and use the Stokes vectors to calculate the polarimetric parameters: the angle of polarization (AOP, θ), based on formula of AOP describing the degree of polarization (DOP, ρ). Then, we estimate the atmospheric light value at infinity (A_∞) based on the average total intensity in RGB channel, and re-construct a matrix to estimate the global transmission map ($t(z)$). Finally, haze-free images have been obtained by atmospheric scattering model. Experimental results show that our method can more accurately estimate the atmospheric light value at infinity and the medium transmittance, and the dehazed image has high contrast and visibility.

2. Related work and technique

2.1. Atmospheric scattering model

The atmospheric scattering model [19] as widely used to describe haze-related irradiance reflected from the scene and its detection by image acquisition devices. The model can be expressed as

$$I = D + A \tag{1}$$

where I is the observed intensity; D is the direct light reflected from the detected object(s); A is the air light scattered from the haze particles. Therefore, $I$and D can be expressed as

$$D = L^{obj}t(z) \tag{2}$$

$$A = A_\infty(1 - t(z)) \tag{3}$$

where L^{obj} is the scene radiance, without attenuation by the haze; A_∞ is the air light from an object at infinity; t is the medium transmission describing the portion of the light that was not scattered and reaches the camera. We assume that the atmosphere is homogeneous, and that $t(z)$ can be expressed as

$$t(z) = e^{-\beta z} \tag{4}$$

Where β is the scattering coefficient of the atmosphere; Z is the scene depth. Our model assumes that the extinction coefficient is distance-invariant. Therefore, the atmospheric scattering model can be expressed as

$$I = L^{obj}t(z) - A_\infty(1 - t(z)) \tag{5}$$

Corresponding to Eq. (5), the final haze-free image L^{obj} can be expressed as

$$L^{obj} = \frac{I - A}{1 - A/A_\infty} \tag{6}$$

From Eq. (6), air light from an object at an infinite distance A_∞ and the medium transmission $t(z)$ are the key parameters for acquiring the final haze-free image. Based on the polarimetric information, the two key parameters were accurately estimated, as described below.

2.2. Stokes vectors

Atmospheric particles and objects in the scene undergo partial polarization, and a common representation of the polarization state is the Stokes vector representation [20,21] $S = [S_0, S_1, S_2, S_3]^T S_0$ represents the total intensity of the remitted and collected light; S_1 represents the difference between the horizontal and vertical linearly polarized components, and S_2 represents the difference between the 45° and 135° linearly polarized components, respectively; S_3 represents the circularly polarized light component. The circularly polarized component of polarized light is quite small; thus, it is neglected. We place a linear polarizer in front of a detector. After that, we rotate the linear polarizer at four angles of 0°, 45°, 90°, and 135°, to capture four polarimetric images, whose intensities are represented as $I(0)I(45)I(90)I(135)$. Thus, the Stokes vector can be expressed as [21]

$$S = \begin{bmatrix} S_0 \\ S_1 \\ S_2 \end{bmatrix} = \begin{bmatrix} I(0) + I(90) \\ I(0) - I(90) \\ I(45) - I(135) \end{bmatrix} \tag{7}$$

From Eq. (7), the (DOP, ρ) and (AOP, θ) are given by

$$\rho_{(x,y)} \underset{c\in\{r,g,b\}}{=} \frac{\sqrt{(S^c_{1(x,y)})^2 + (S^c_{2(x,y)})^2}}{S^c_{0(x,y)}}. \tag{8}$$

$$\theta_{(x,y)} \underset{c\in\{r,g,b\}}{=} \frac{1}{2}\arctan\left(\frac{S^c_{2(x,y)}}{S^c_{1(x,y)}}\right). \tag{9}$$

Here, we calculate ρ and θ for each pixel.

2.3. Estimation of A_∞ and $t(z)$

Precise estimation of A_∞ and $t(z)$ is the most important factor that determines the quality of the dehazed image. In our approach, direct light is assumed to be non-polarized, because direct light can be depolarized owing to the presence of atmospheric particles [1]. Therefore, the polarization of a hazy image can be mainly expressed by air light. In previous studies, air light estimation depended on the presence of sky regions in images, which poses a challenge for high-brightness object without sky regions.

In Eq. (9), AOP dependents the S_1 and S_2, so it is disturbed mainly in polarized light. Therefore, AOP has its advantage, it can provide much more precise information of the airlight compared with DOP, and we adopt the highest frequency as the AOP of airlight in each color channel, which is defined as θ_m. Then, we estimate the ρ based on θ_m, from Eqs. (8) and (9), ρ can be derived as:

$$\rho_{(x,y)} \underset{c\in\{r,g,b\}}{=} \frac{S^c_{1(x,y)}\sqrt{(1+\tan^2(2\theta_m))}}{S^c_{0(x,y)}} \tag{10}$$

DOP of the airlight (ρ_A) is determined from the matrix elements of ρ, and ρ_A can be estimated as the lagest value among the maxtrix. Therefore, A can be expressed as $A = A_p/\rho_A$, where A_p is the irradiance of the polarized part of the airlight, and the DOP of the total radiance as $\rho = A_p/S_0$. It is easily to derive A from Eq. (10) as

$$A_{(x,y)} \underset{c\in\{r,g,b\}}{=} \frac{S^c_{1(x,y)}\sec(2\theta_m)}{\rho_A} \tag{11}$$

In fact, $e^{-\beta z}$ is approximately equal to zero, due to estimating the distance Z of the sky area is deemed as infinity, in this case, from Eq. (3), we can find that A_∞ is equal to A. In other words, A includeds in A_∞accordance with $A = A_p/\rho_A$, and therefore A_∞ can be directly estimated from A by choosing the maximum value [22]. However, this scheme estimating A_∞ is not precise, some pixels will be black and add noise in dehazed image when A_∞ equal to elements of matrix A. Accordingly, estimating the optimal A_∞ is the most important. The spatial variation of A_∞ depends on the position of sun relative to viewing dircetion, due to strong forward scattering and backscattering, A_∞ will usually be larger when the Sun is in front or behind the camera [1]. According to Eq. (5), we can see that with A_∞ changes, the total intensity I changes accordingly. Because of the position of Sun and the size of scattering particles, the scenes and sky region has different performance in raw image, it means that the quality of dehazed image realtive to the brightness of raw image. Thus, we consider averaging the raw image pixels of each color channel, and re-estimating the optimal A_∞. They can be expressed as

$$\alpha = \frac{1}{3\times M\times N}\sum_{x=1}^{M}\sum_{y=1}^{N}(I_r(x,y)+I_g(x,y)+I_b(x,y)) \tag{12}$$

where α is average intensity of raw image, $M\times N$ is the size of image, $I_r(x,y)$, $I_g(x,y)$, $I_b(x,y)$is Red channel, Green channel, Blue channel, respectively. We note that the total intensity includes$A$, θ_m is the polarized direction of A, we can derived that$I = A/\cos\theta_m$, A_∞ can be approximately estimated by using the following expression

$$|A_\infty| = a\cos\theta_m \tag{13}$$

In generally, the different scenes of dehazed image have dark or white region, because of choosing the brightness pixel of sky region as A_∞. This scenario based on the information of AOP of airlight and the average intensity which can reduce the error of choosing one brightness pixel as A_∞ or estimating A_∞ by maximum value of A. In Ref. [22], Liang et al. had caculated and constructed an imaginary matrix T:

$$T = \frac{2I_{0(x,y)}}{1+\rho_A\cdot\cos 2\theta_m} \tag{14}$$

where ρ_A is DOP of the airlight, θ_m is the highest frequency of AOP of airlight, they checking the elements of T and find the one which is closest to total intensity, this value had been regarded as the airlight radiance from the infinite distance A_∞. This imaginary matrix is only under the condition that distance Z is infinity. Based on this matrix, we re-constructed a image similar to the transmission$t(z)$. The optimal $t(z)$ is related to precisely estimate the scattering coefficient β and the scene depth Z, which are difficult to estimate. In our experiment, we find that the image of T has the high intensity in the sky region(approximately equal to infinity) and minimum intensity of the scenes. This map is opposite to the $t(z)$, according to matrix T, one can derive the expression of $t(z)$:

$$\hat{t}(z)_{(x,y)} = \frac{1}{T_{(x,y)}} \tag{15}$$

Because of the large jumps along edges, an incorrect halo will appears. In this case, to estimate $t(z)$by each pixel, one can reduce or even eliminate halo. Besides, this scenario is more convenient and faster than filtering algorithms. Thus, the dehazing algorithm consists of three main steps. Fig. 1 shows the flowchart of our dehazing algorithm: (1) Acquire polarimetric images with different orientations; (2) Based on Stokes vectors to calculate the ρ and θ, then estimating the infinity airlight A_∞ and the transmission map $t(z)$; (3) Combine the atmospheric scattering model to remove haze.

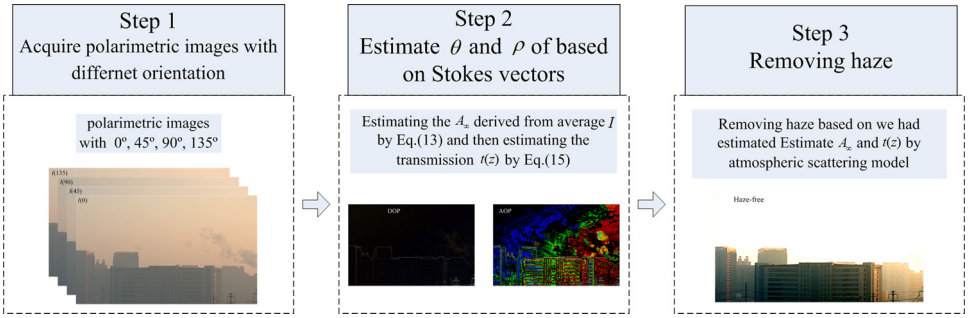

Fig. 1. Flowchart of our dehazing algorithm.

3. Experiment result

In this study, we tested whether our scheme can enhance the visibility of scenes, correct the color shift, and retain detail-related information effectively in the presence of haze. The experimental setup is shown in Fig. 2, the images was taken by a HD network camera (image size is 1920 × 1080) equipped with a lens that we had designed (f: 2.4, focal length: 30 mm, field of view: 13°), we placed a rotating disc mounted with linearly polarizing filters with four different polarization axes (0°, 45°, 90° and 135°) in front of camera lens.

The first step of our experiment, we rotated the linear polarizer at four angles to capture four polarimetric images and obtained three groups of typical images. Fig. 3 shows different scenes for different hazy weather conditions. Fig. 3(a) and (b) shows the sky regions illuminated by sunlight, and the scenes (mirror) reflects the sunlight partially. This condition will erroneous estimate infinite atmospheric light caused some pixels more brightness than sky region. Fig. 3(c) shows overcast weather and thick haze, this image has lower contrast and color fidelity. Next, we used the MATLAB 2014a package, which runs on an Intel(R) Core(TM) 3.2-GHz CPU with 8GB of RAM, and processing the polarimetric images.

The next step is to process images by the polarimetric information introduced in Section 2. The average total intensity is shown in Table 1, and based on Eq. (15), the transmission maps $t(z)$ are shown in Fig. 4. In Fig. 4(a), the distance between the nearest building and the camera is about 0.9 km, the distance between farthest building and camera is 1.8 km. In Fig. 4(b), the distance between the nearest building and the camera is about 0.9 km, the distance between farthest building and camera is 1.5 km. In Fig. 4(c) the distance between the nearest building and the camera is about 0.75 km, the distance between farthest building and camera is 1.2 km. From Eq. (4), we assume that the scattering coefficient is constant, therefore the transmission $t(z)$ decreased with the distance increased. In Fig. 4, scene at different distance (depth) of the transmission map $t(z)$, as can be seen, the estimated $t(z)$ have lighter color in free-haze regions while having darker color in dense-haze regions as expected. Therefore, estimating the transmission map$t(z)$ can be verified accuracy.

After estimating the transmission map $t(z)$ and infinity airlight A_∞, we verified that our method can unveil more details and recover real color in different weather condition. The dehazing results are shown in Fig. 5. In Fig. 5, the original hazy images have low contrast, and detailed information is difficult to resolve, but the recovered images have more detail-related information and feature correct color fidelity. For Scene 1, we compared the original image (a) and the recovered image (b). The red region in image (a) at the top of a tall building has a plaque, whose characteristics and the building outline are difficult to resolve. As for the red region in the dehazed image (b), the plaque characteristic and the building outline are more easily resolved, especially when comparing between (a-1), (a-2) and (b-1), (b-2) for the region outlined by the red rectangle. For Scene 2, the image in (c) loses color fidelity and has degraded visibility owing to the haze; the recovered image in (d) reveals the inherent color and better visibility. In the

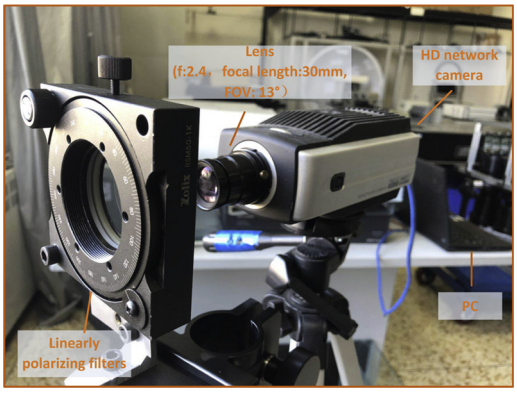

Fig. 2. Experimental setup.

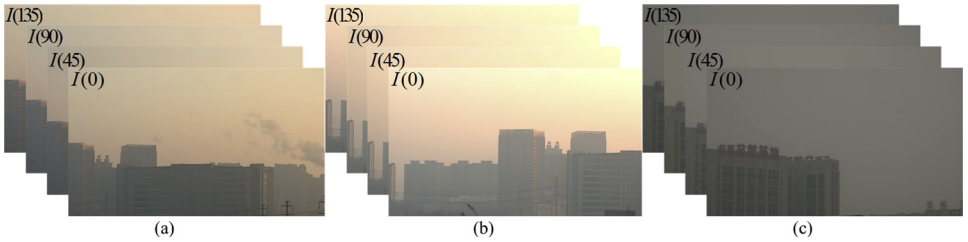

Fig. 3. Three typical polarimetric images, for different hazy weather conditions, without any additional processing.

Table 1
Three typical images of the average intensity value.

	Image 1	Image 2	Image 3
α	1.2501 1.5635	1.4693 2.1588	1.0275 1.0520

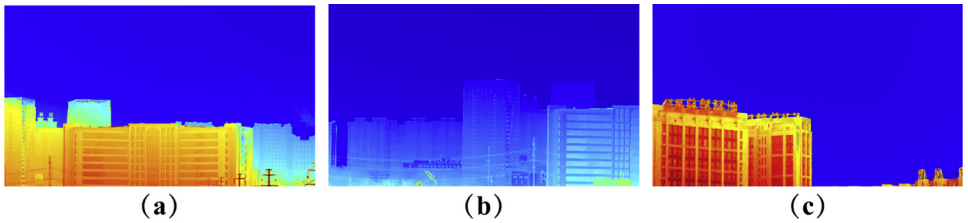

Fig. 4. Obtaining the transmission maps by our method.

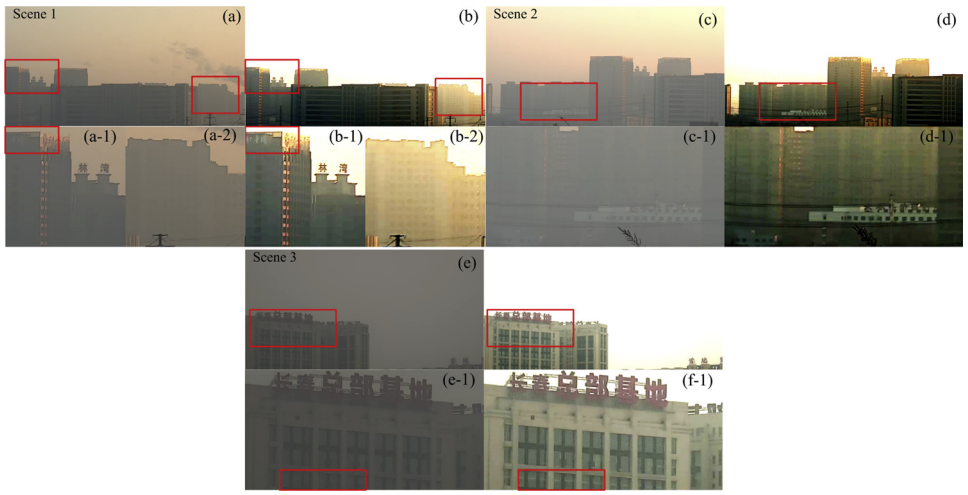

Fig. 5. Original images of different scenes, dehazed images, and details; (a), (c), and (e) are the original hazy images; (b), (d), and (f) are the dehazed images; the other images show the comparison of the original and dehazed images in detail.

red rectangle region in the images in (c) and (d) and enlarged images in (c-1) and (d-1) of this region, the recovered image not only has a corrected color shift, but also reveals many details and structures. In Scene 3, the original image in (e) has low intensity, and the scenes do not contain specific information and do not feature the true color. The recovered image in (f) shows that the color is corrected and more details are recovered, in particular in the red rectangle region of the images in (e-1) and (f-1).

To further evaluate the effectiveness of the proposed method, we evaluated image quality in terms of the ratio between the gradients at visible edges [23]. The edge number indicates the number of visible edges in the restored images; Fig. 6 shows that the restored images have more edges than the original images; thus, our scheme can recover more details and enhances visibility. Then, we compared the distributions of the RGB color components. In Fig. 7, the original image has lower RGB number than the recovered image. Therefore, the recovered image has richer color palette than the hazy image, which confirms that our method can correct the color shift. Depending on the objective, we conclude that our method can not only recover more details, but also restore the true

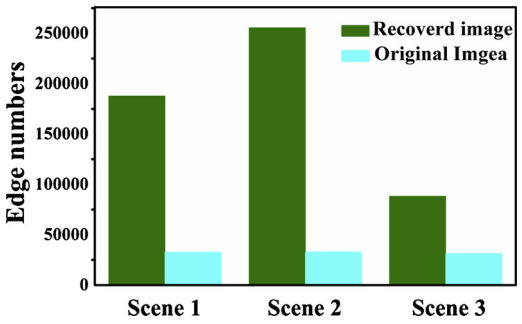

Fig. 6. Comparison of the original and restored images in terms of their edge numbers.

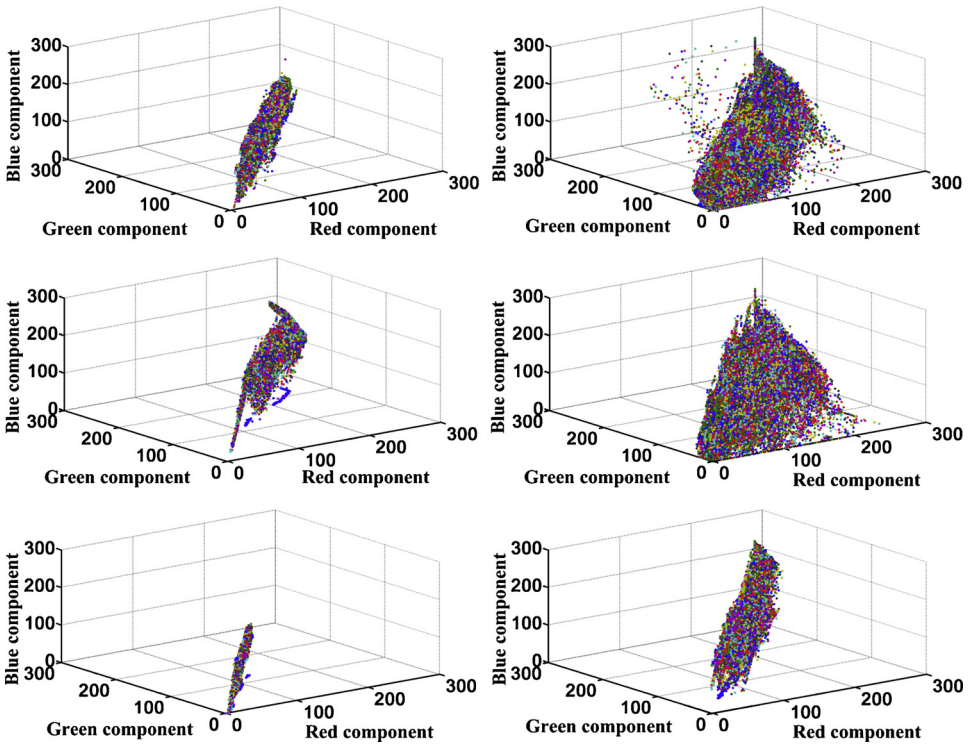

Fig. 7. Comparison of the distributions in the RGB color space; (a-1), (b-1), and (c-1) are the hazy images, (a-2), (b-2), and (c-2) are the restored images.

color.

4. Conclusion

In this paper, we used polarimetric method to removal haze, this is a simple and convenient method. Based on polarimetric information in each pixels of four orientation images to estimate the infinite atmospheric light value A_{∞}, and re-construct a matrix to precisely estimate transmission map $t(z)$, subsequently through atmospheric scattering model to recover the image. Although this method based on polarimetric parameters, it has the advantage of enhancing robustly such degraded images. Experimental results show that this technique can enhance visibility, unveil more details, capture the sharp edge discontinuities and outline the profile of the objects. Also, this technique can correct the color fidelity and recover the image faithfully. Because of the size of image is 1980×1080, finally we acquired a haze-free image that will cost about 4 s.

Moreover, our experiment scheme has two weakness, one is need four orientation polarimetric images, so acquiring simultaneous haze-free image was limited by the camera, the other is we also need to keep the camera stable in order to avoid the pixel mislocation of the different orientation polarimetric image. Therefore, in the future, we will use the camera with four polarimetric orientations to simultaneously acquire images, which can be applied in removing haze that include the dynamic targets.

Acknowledgements

Project supported by Fundamental Research Funds of the State Key Laboratory of Applied Optics, CIOMP (Changchun Institute of Optics, Fine mechanics and Physics, Chinese Academy of Sciences).

References

[1] Y.Y. Schechner, S.G. Narasimhan, S.K. Nayar, Polarization-based vision through haze, Appl. Opt. 42 (2003) 511–525.
[2] E. Namer, S. Shwartz, Y.Y. Schechner, Skyless polarimetric calibration and visibility enhancement, Opt. Express 17 (2009) 472–493.
[3] J. Mudge, M. Virgen, Real time polarimetric dehazing, Appl. Opt. 52 (2013) 1932–1938.
[4] S. Fang, X. Xia, X. Huo, C. Chen, Image dehazing using polarization effects of objects and airlight, Opt. Express 22 (2014) 19523–19537.
[5] Y. Lu, M. Xu, S. Jia, W. Huang, Fast snow removal algorithm based on the maximum value of the degree of polarization and angle of polarization, Phys. Scr. 94 (2019).
[6] H. Tian, J. Zhu, S. Tan, Y. Zhang, Y. Zhang, Y. Li, X. Hou, Rapid underwater target enhancement method based on polarimetric imaging, Opt. Laser Technol. 108 (2018) 515–520.
[7] Y. Qu, Z. Zou, Non-sky polarization-based dehazing algorithm for non-specular objects using polarization difference and global scene feature, Opt. Express 25 (2017) 25004–25022.
[8] W. Zhang, J. Liang, L. Ren, H. Ju, E. Qu, Z. Bai, Y. Tang, Z. Wu, Real-time image haze removal using an aperture-division polarimetric camera, Appl. Opt. 56 (2017) 942.
[9] J. Liang, L. Ren, H. Ju, W. Zhang, E. Qu, Polarimetric dehazing method for dense haze removal based on distribution analysis of angle of polarization, Opt. Express 23 (2015) 26146–26157.
[10] J. Li, Y. Li, Underwater image restoration algorithm for free-ascending deep-sea tripods, Opt. Laser Technol. 110 (2019) 129–134.
[11] J. Lu, N. Li, S. Zhang, Z. Yu, H. Zheng, B. Zheng, Multi-scale adversarial network for underwater image restoration, Opt. Laser Technol. 110 (2018).
[12] K. He, J. Sun, X. Tang, Single image haze removal using dark channel prior, IEEE Trans. Pattern Anal. 33 (2011) 2341–2353.
[13] D. Berman, T. Treibitz, S. Avidan, Non-local image dehazing, 2016 IEEE Conference on Computer Vision and Pattern Recognition (CVPR) (2016) 1674–1682.
[14] J. Tarel, N. Hautière, Fast visibility restoration from a single color or gray level image, 2009 IEEE 12th International Conference on Computer Vision (2009) 2201–2208.
[15] C.-H. Yeh, L.-W. Kang, M.-S. Lee, C.-Y. Lin, Haze effect removal from image via haze density estimation in optical model, Opt. Express 21 (2013) 27127–27141.
[16] R. Fattal, Single image dehazing, ACM Trans. Graph. (TOG) 27 (2008) 72.
[17] R.T. Tan, Visibility in bad weather from a single image, 2008 IEEE Conference on Computer Vision and Pattern Recognition, IEEE (2008) 1–8.
[18] S.K. Nayar, S.G. Narasimhan, Vision in Bad Weather, (1999).
[19] S.G. Narasimhan, S.K. Nayar, Vision and the atmosphere, Int. J. Comput. Vision 48 (2002) 233–254.
[20] D.H. Goldstein, Polarized Light, Revised and Expanded, CRC press, Boca Raton, 2003.
[21] M. Bass, E. Van Stryland, D.R. Williams, W.L. Wolfe, Handbook of Optics Volume II Devices, Measurements, and Properties, 2nd edition, McGraw-Hill, New York, 1995.
[22] J. Liang, L. Ren, H. Ju, E. Qu, Y. Wang, Visibility enhancement of hazy images based on a universal polarimetric imaging method, J. Appl. Phys. 116 (2014) 173107.
[23] N. Hautiere, J.-P. Tarel, D. Aubert, E. Dumont, Blind contrast enhancement assessment by gradient ratioing at visible edges, Image Anal. Stereol. 27 (2011) 87–95.